0090-9556/08/3607-1267–1274$20.00
DRUG METABOLISM AND DISPOSITION
Copyright © 2008 by The American Society for Pharmacology and Experimental Therapeutics
DMD 36:1267–1274, 2008

Vol. 36, No. 7
19711/3347844
Printed in U.S.A.

Pharmacokinetic-Pharmacodynamic Modeling of Biomarker Response and Tumor Growth Inhibition to an Orally Available cMet Kinase Inhibitor in Human Tumor Xenograft Mouse Models

Shinji Yamazaki, Judith Skaptason, David Romero, Joseph H. Lee, Helen Y. Zou, James G. Christensen, Jeffrey R. Koup, Bill J. Smith, and Tatiana Koudriakova

Pfizer Global Research and Development, La Jolla Laboratories, San Diego, California (S.Y., J.S., D.R., J.H.L., H.Y.Z., J.G.C., B.J.S., T.K.); and Pfizer Global Research and Development, Ann Arbor Laboratories, Ann Arbor, Michigan (J.R.K.)

Received November 12, 2007; accepted March 31, 2008

ABSTRACT:

(*R*)-3-[1-(2,6-Dichloro-3-fluoro-phenyl)-ethoxy]-5-(1-piperidin-4-yl-1*H*-pyrazol-4-yl)-pyridin-2-ylamine (PF02341066) was identified as an orally available, ATP-competitive small molecule inhibitor of cMet receptor tyrosine kinase. The objectives of the present studies were to characterize 1) the pharmacokinetic-pharmacodynamic relationship of the plasma concentrations of PF02341066 to cMet phosphorylation in tumor (biomarker) and 2) the relationship of cMet phosphorylation to antitumor efficacy (pharmacological response). Athymic mice implanted with GTL16 gastric carcinoma or U87MG glioblastoma xenografts were treated with PF02341066 once daily at doses selected to encompass ED_{50} values. Plasma concentrations of PF02341066 were best described by a one-compartment pharmacokinetic model. A time-delay (hysteresis) was observed between the plasma concentrations of PF02341066 and the cMet phosphorylation response. A link model was therefore used to account for this hysteresis. The model fitted the time courses of cMet phosphorylation well, suggesting that the main reason for the hysteresis is a rate-limiting distribution from plasma into tumor. The EC_{50} and EC_{90} values were estimated to be 19 and 167 ng/ml, respectively. For tumor growth inhibition, the exponential tumor growth model fitted the time courses of individual tumor growth inhibition well. The EC_{50} for the GTL16 tumor growth inhibition was estimated to be 213 ng/ml. Thus, the EC_{90} for the inhibition of cMet phosphorylation corresponded to the EC_{50} for the tumor growth inhibition, suggesting that near-complete inhibition of cMet phosphorylation (>90%) is required to significantly inhibit tumor growth (>50%). The present results will be helpful in determining the appropriate dosing regimen and in guiding dose escalation to rapidly achieve efficacious systemic exposure in the clinic.

Pharmacokinetic-pharmacodynamic (PKPD) modeling is increasingly being applied in drug discovery and development. Specific applications include 1) the selection of drug candidates with most favorable PKPD properties and 2) the prediction of exposure response in patients with the aim of optimizing the design of early clinical trials. The increased understanding of drug action derived from PKPD-based drug development leads to more information, especially with regard to the identification of drug dosage regimen that results in optimal therapeutic outcome (Derendorf et al., 2000; Lesko et al., 2000; Chien et al., 2005). The use of PKPD modeling in this context relies on prediction of the time course of drug effects in patients, using information from preclinical investigation. Preclinical studies are useful alternatives to investigate PKPD relationships to get insight into the in vivo mechanism of drug action. The integration of PKPD modeling and simulation in drug development has provided opportunities to accelerate the evaluation of new chemical entities in the clinic. Thus, the PKPD investigation could contribute to shortening the overall period of drug development.

Article, publication date, and citation information can be found at http://dmd.aspetjournals.org.
doi:10.1124/dmd.107.019711.

The cMet receptor tyrosine kinase and its ligand, hepatocyte growth factor (HGF), are highly expressed relative to surrounding tissue in numerous cancers, and their expression correlates with poor patient prognosis (Birchmeier et al., 2003). Cell lines engineered to express high levels of cMet and HGF receptor (autocrine loop) or mutant cMet displayed a proliferative, motogenic, and/or invasive phenotype and grew as metastatic tumors in nude mice (Rong et al., 1992, 1994; Bellusci et al., 1994; Jeffers et al., 1997). Thus, cMet and HGF have been implicated in the development and progression of multiple human cancers and are attractive targets for cancer therapy. PF02341066 (Fig. 1), was identified as an orally available, ATP-competitive small molecule inhibitor of cMet kinase (K_i 4 nM) (Zou et al., 2007). PF02341066 was selective for cMet (and anaplastic lymphoma kinase) compared with a panel of >120 diverse tyrosine and serine-threonine kinases. PF02341066 potently inhibited in vitro cMet phosphorylation and signal transduction as well as cMet-dependent proliferation, migration, or invasion of human tumor cells (IC_{50} values: 5–20 nM). In addition, PF02341066 potently inhibited HGF-stimulated endothelial cell survival and invasion or serum-stimulated endothelial cell tubulogenesis in vitro, suggesting that this compound also exhibits antiangiogenic properties (Zou et al., 2007).

ABBREVIATIONS: PKPD, pharmacokinetic-pharmacodynamic; HGF, hepatocyte growth factor; PF02341066, (*R*)-3-[1-(2,6-dichloro-3-fluoro-phenyl)-ethoxy]-5-(1-piperidin-4-yl-1*H*-pyrazol-4-yl)-pyridin-2-ylamine; HPLC, high-performance liquid chromatography.

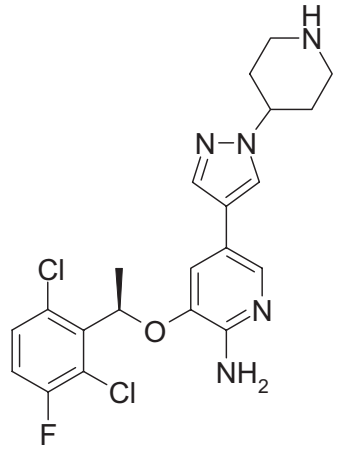

FIG. 1. Chemical structure of PF02341066 [(*R*)-3-[1-(2,6-dichloro-3-fluoro-phenyl)-ethoxy]-5-(1-piperidin-4-yl-1*H*-pyrazol-4-yl)-pyridin-2-ylamine].

The application of PKPD principles and procedures to the rational development of PF02341066 will be essential. The objectives of the present studies were to characterize 1) the PKPD relationship of PF02341066 plasma concentrations to cMet phosphorylation in tumors (biomarker) and 2) the relationship of cMet phosphorylation to antitumor efficacy (pharmacological response) in athymic mice implanted with human tumor xenografts. The extrapolation of the present PKPD relationships to patients using the combination of in vitro and in vivo data can be particularly helpful in determining the appropriate dosing regimen in clinical studies and in guiding dose escalation to achieve systemic exposure in patients who are expected to have pharmacological effects.

Materials and Methods

Chemicals. PF02341066 (hydrochloride salt: chemical purity >99%) and a structurally related in-house compound (internal standard for analysis) were synthesized by Pfizer Global Research and Development (San Diego, CA). All other commercially available reagents and solvents were of either analytical or high-performance liquid chromatography (HPLC) grade.

In Vivo PKPD Study. Detailed information about in vivo PKPD studies was reported previously by Zou et al. (2007). In brief, three separate repeated oral-dose PKPD studies were conducted with PF02341066 in athymic mice implanted with GTL16 gastric carcinoma or U87MG glioblastoma xenografts (studies 1–3). Mice were treated with PF02341066 for 9 to 11 days at selected doses. A subset of mice was humanely euthanized at 1, 4, 8, and 24 h after the last dosing. Blood samples (n = 3/time point) were collected by exsanguination via cardiac puncture to determine plasma concentration of PF02341066 (studies 1–3). Resected tumors (n = 3/time point) were snap-frozen and pulverized using a liquid nitrogen-cooled cryomortar and pestle, and protein lysates were generated. The level of total phosphorylated tyrosine protein in the cMet receptor (cMet phosphorylation) was determined using a capture enzyme-linked immunosorbent assay method (studies 1 and 2). Tumor volume was also measured during the treatment period (studies 1–3) by electronic Vernier calipers and was calculated as the product of its length × width^2 × 0.4. Dose levels of each study were summarized as follows: 1) study 1 (GTL16 xenograft model) at 8.5, 17, and 34 mg/kg; 2) study 2 (GTL16 xenograft model) at 3.13, 6.25, 12.5, 25, and 50 mg/kg; and 3) study 3 (U87MG xenograft model) at 3.13, 6.25, 12.5, 25, and 50 mg/kg. All of the procedures were conducted in accordance with the Institute for Laboratory Animal Research Guide for the Care and Use of Laboratory Animals and with Pfizer Animal Care and Use Committee guidelines.

PF02341066 Analysis. Plasma concentrations of PF02341066 were quantitatively determined by liquid chromatography-tandem mass spectrometry. Mouse plasma samples were extracted with a methanol-acetonitrile mixture (1:1, v/v). Chromatography was performed with an HP1100 HPLC system (Agilent Technologies, Palo Alto, CA) using a reverse-phase column (XDB-C18, 2.1 × 50 mm, 5 μm; Agilent Technologies). Mass spectrometric analysis was performed on a Quattro Ultima triple-stage quadrupole mass spectrometer (Micromass; Waters, Beverly, MA) using electrospray ionization. The mobile phase consisted of A (98% HPLC grade water, 2% acetonitrile, and 0.1% formic acid) and B (98% acetonitrile, 2% HPLC grade water, and 0.1% formic acid) at a flow rate of 0.4 ml/min. The gradient elution was programmed from 5 to 60% B over 2.5 min. The mass spectrometer was operated under the following conditions: capillary voltage 2.5 kV, cone voltage 45 V, source temperature 120°C, and dissolution temperature = 350°C. Sample analysis was performed in the positive ionization multiple reaction monitoring mode with unit resolution for the transitions of m/z 450 to 260 for PF02341066 and m/z 377 to 348 for the internal standard. Total time for the analytical run was 4.6 min. Data were processed using Masslynx 3.5 software (Micromass). The calibration curve range was 1 to 2500 ng/ml. The back-calculated calibration standard concentrations were within ±15% of their theoretical concentrations with coefficients of variation of less than 12%. The precision and accuracy of the quality control samples were within ±14%.

In Vitro Plasma Protein Binding. The plasma free fraction of PF02341066 was determined in mouse plasma at 0.23 to 9 μg/ml (0.5–20 μM) using the equilibrium dialysis technique. The study was conducted in a 96-well Teflon dialysis chamber (HTDialysis LLC, Gales Ferry, CT) using a semipermeable membrane (Spectra/Por4; Spectrum, Laguna Hills, CA) with a 12,000 to 14,000 Da molecular mass cut-off. An aliquot of plasma (0.15 ml) was placed in half the well in triplicate. The second half of the well contained an equal volume of potassium buffer (100 mM, pH 7.4). The plate was covered with a top seal film to avoid evaporation and incubated at 37°C for 6 h. Pilot experiments revealed that 1) PF02341066 was stable in plasma and 2) protein binding reached equilibrium at 37°C for 6 h. After incubation, the plasma (0.02 ml) and buffer (0.08 ml) were transferred to separate tubes containing either 0.08 ml of blank buffer or 0.02 ml of blank plasma, respectively. Samples were extracted with 0.3 ml of an acetonitrile-methanol mixture (1:1, v/v) containing the internal standard and analyzed by liquid chromatography-tandem mass spectrometry as described above. The free fraction (f_u) was calculated by the equation $f_u = C_{buffer}/C_{plasma}$, where C_{buffer} and C_{plasma} denote the concentrations of PF02341066 in buffer and plasma, respectively, after the incubation.

Pharmacokinetic Analysis. A naive-pooled pharmacokinetic analysis was used to determine pharmacokinetic parameters of PF02341066 in mice because a subset of mice (n = 3/time points) was humanely euthanized at each time point to collect blood samples. Therefore, all individual data at each dose were pooled together for the pharmacokinetic analysis as if they came from a single individual (Sheiner, 1984). Pharmacokinetic analysis was performed with a standard one-compartment linear model with a first-order absorption rate as implemented in NONMEM version V (University of California at San Francisco, San Francisco, CA) (Beal and Sheiner, 1992). The subroutine ADVAN2 with TRANS2 was used for the NONMEM analysis. This model was parameterized using absorption rate constant (k_a, hours^{-1}), oral clearance (CL/F, liters per hour per kilogram), and oral volume of distribution (Vd/F, liters per kilogram). Residual variability was characterized by a proportional error model. Pharmacokinetic parameters obtained were used to simulate plasma concentrations as a function of time after oral dose administration to drive the time-dependent pharmacodynamic model.

PKPD Modeling. The response of cMet phosphorylation in tumor to a plasma concentration of PF02341066 was modeled using a link model (an effect-compartment model) (Sheiner et al., 1979) and an indirect response model (Dayneka et al., 1993; Jusko and Ko, 1994). In brief, the effect site concentration of PF02341066 (C_e, nanograms per milliliter) was expressed by the following differential equation:

$$\frac{dC_e}{dt} = k_{e0} \cdot (C_p - C_e)$$

where k_{e0} is the rate constant (hours^{-1}) for equilibration with the effect site and C_p is the plasma concentration of PF02341066 (nanograms per milliliter).

In the link model, the following equation was used to determine EC_{50} (the concentration causing one-half maximum effect, E_{max}) for the inhibition of cMet phosphorylation (E):

$$E = E_0 \times \left(1 - \frac{E_{max} \times C_e^{\gamma}}{EC_{50}^{\gamma} + C_e^{\gamma}}\right)$$

where E_0 is the baseline of cMet phosphorylation and γ is the Hill coefficient.

An indirect response model assumes that cMet phosphorylation is maintained by the balance of formation and degradation rates. PF02341066 is considered to inhibit the formation rate because PF02341066 is a competitive ATP-binding inhibitor of cMet kinase. Therefore, the following differential equation was used to determine EC_{50} for the inhibition of cMet phosphorylation (R):

$$\frac{dR}{dt} = k_{in} \cdot \left(1 - \frac{E_{max} \times C_p^{\gamma}}{EC_{50}^{\gamma} + C_p^{\gamma}}\right) - k_{out} \cdot R$$

where k_{in} is the zero-order formation rate constant (hours^{-1}) and k_{out} is the first-order degradation rate constant (hours^{-1}).

Furthermore, an indirect response model with the effect compartment, that is, C_e instead of C_p, was performed to determine EC_{50} for the inhibition of cMet phosphorylation (R):

$$\frac{dR}{dt} = k_{in} \cdot \left(1 - \frac{E_{max} \times C_e^{\gamma}}{EC_{50}^{\gamma} + C_e^{\gamma}}\right) - k_{out} \cdot R$$

In vivo tumor growth in xenograft models is known to follow exponential growth, at least in its early phases. Subsequently, the tumor volume follows a linear growth, eventually reaching a plateau (Gompertz, 1825; Bissery et al., 1996). This behavior can be described using a Gompertz model (Gompertz, 1825). In our approach, the tumor growth curves in control groups were first modeled by an exponential tumor growth model in which tumor volume inhibits the growth rate:

$$\frac{dT}{dt} = k_{in} \cdot \left(1 - \frac{T}{TG_{50} + T}\right) \cdot T - k_{out} \cdot T$$

where T is tumor volume, k_{in} is the first-order tumor growth rate constant (hours^{-1}), TG_{50} is the tumor volume that inhibits 50% of the tumor growth rate, and k_{out} is the first-order tumor loss rate constant (hours^{-1}).

The response of tumor volume (T) to plasma concentration of PF02341066 was then modeled using an exponential tumor growth model including inhibition of the growth rate by both tumor volume and PF02341066 concentration:

$$\frac{dT}{dt} = k_{in} \cdot \left(1 - \frac{T}{TG_{50} + T}\right) \cdot \left(1 - \frac{E_{max} \times C_p^{\gamma}}{EC_{50}^{\gamma} + C_p^{\gamma}}\right) \cdot T - k_{out} \cdot T$$

In many in house studies, the estimates of TG_{50} values in control groups were greater than the observed maximum tumor volumes, suggesting that tumor growth simply followed the exponential growth curve in a study period. Therefore, the above tumor model in the control group could be simplified to the following differential equation:

$$\frac{dT}{dt} = k_{in} \cdot T - k_{out} \cdot T$$

The response of tumor volume (T) to plasma concentration of PF02341066 was then modeled by the following differential equation:

$$\frac{dT}{dt} = k_{in} \cdot \left(1 - \frac{E_{max} \times C_p^{\gamma}}{EC_{50}^{\gamma} + C_p^{\gamma}}\right) \cdot T - k_{out} \cdot T$$

All analyses were performed with NONMEM version V and *S*-Plus 6.2 (Insightful Corporation, Seattle, WA). The NONMEM subroutine ADVAN6 was used for the link model, whereas the ADVAN8 was used for the indirect response model and the tumor growth inhibition model. The Hill coefficient (γ) was fixed to be unity in all PKPD models. The initial conditions at time 0 for the gastrointestinal tract compartment, cMet phosphorylation, and tumor volume were the dose amount (milligrams per kilogram), the mean cMet phosphorylation ratio of control animals (i.e., unity), and the individual tumor volume (cubic millimeters), respectively. Residual variability was characterized by a proportional error model. In the exponential tumor growth model with a population analysis, an interanimal variability for k_{out} was estimated using an exponential variance model. Model selection was based on a number of criteria such as the objective function value, estimates, standard errors, and scientific plausibility and exploratory analysis of the goodness-of-fit plots. The difference in the objective function between two nested models was compared with a χ^2 distribution in which a difference of 6.63 was significant at the 1% level. The final models were validated by running a bootstrap validation procedure with 5000 data sets (Efron and Tibshirani, 1993). The parametric statistics of the parameters (median and 10th and 90th percentiles) generated were compared with the final parameter estimates generated by the NONMEM analysis.

Results

Pharmacokinetics. The unbound fractions of PF02341066 in mouse plasma (0.030–0.033) were concentration-independent at 0.23 to 9 μg/ml (0.5–20 μM). The majority of plasma concentrations of PF02341066 at the lowest dose of 3.13 mg/kg were below the lower limit of quantitation (<1 ng/ml). Therefore, pharmacokinetic analysis at the lowest dose was not performed. The observed and model-fitted plasma concentrations of PF02341066 in athymic mice implanted with human tumor xenografts after oral administration are shown in Fig. 2. The pharmacokinetic parameters of PF02341066 are tabulated in Table 1. Plasma concentrations of PF02341066 at the doses of 6.25 to 50 mg/kg in all studies were best described by a one-compartment model with a fixed absorption lag time of 0.8 h. The objective function value for the pharmacokinetic analysis was 1199.5. Pharmacokinetic parameter estimates for k_a, CL/F, and Vd/F were 0.24 to 0.34 h^{-1}, 1.5 to 14 liters/h/kg, and 2.5 to 56 liters/kg, respectively (Table 1). The values of k_a seemed to be independent of the doses. The CL/F and Vd/F values tended to be higher at the lower doses than at the higher doses, suggesting nonlinear pharmacokinetics at the dose range of 6.25 to 50 mg/kg. Preliminary in-house data suggest that nonlinear pharmacokinetics of PF02341066 could be in part due to saturation of hepatic/intestinal clearance at higher doses. The standard errors of each pharmacokinetic parameter were relatively small (coefficient of variation <30%). Residual variability was estimated to be 28%. The final parameter estimates (median values) from the bootstrap validation were 0.23 to 0.33 h^{-1}, 1.5 to 14 liters/h/kg, and 2.5 to 57 liters/kg, respectively. Thus, the final parameter estimates for the bootstrap validation were in good agreement with the estimates of the final pharmacokinetic model (<±3%).

PKPD Relationship. In general, the maximum plasma concentrations were observed at 4 h postdose, whereas the maximum inhibition of cMet phosphorylation was observed at 8 h postdose. Thus, it was apparent that there was a time delay (hysteresis) between plasma concentrations of PF02341066 and the cMet phosphorylation response. The inhibition of cMet phosphorylation was returned to the baseline level at 24 h postdose at the doses of 3.13 and 6.25 mg/kg whereas near-complete inhibition was observed during the dosing interval at the doses of 25 to 50 mg/kg. The observed and model-fitted cMet phosphorylation-time profiles in the GTL16 xenograft model are graphically presented in Fig. 3 (the link model) and Fig. 4 (the indirect response model with the effect compartment). The link model fitted the time profiles of cMet phosphorylation inhibition well. The objective function value was −322. The EC_{50} value was estimated to be 19 ng/ml (Table 2). The calculated EC_{90} value by the Hill equation was 167 ng/ml, which was equivalent to 13 nM free. The indirect response model did not fit the time profiles of cMet phosphorylation inhibition well, especially at the lower doses. This model tended to overpredict the inhibition of cMet phosphorylation and the objective function value was −265. The estimated EC_{50} value was 4.6 ng/ml. By incorporating the effect compartment to the indirect response model, the model fitted the time profiles of cMet phosphorylation inhibition well. The objective function value was −322. The EC_{50} value was

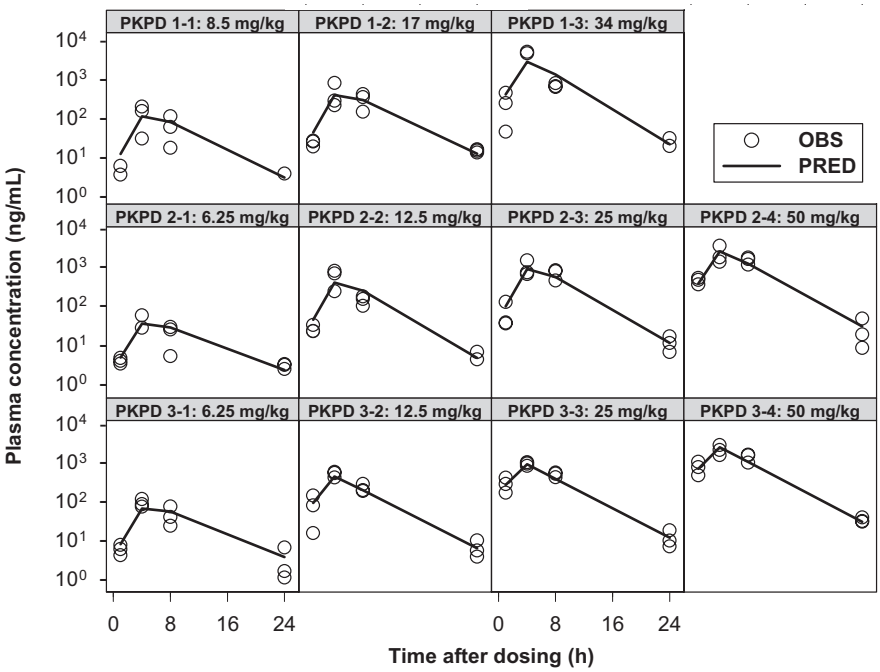

FIG. 2. Observed and model-fitted plasma concentrations of PF02341066 in athymic mice implanted with GTL16 or U87MG xenografts after repeated oral administration of PF02341066. OBS, observed plasma concentrations of PF02341066; PRED, model-fitted plasma concentrations of PF02341066.

TABLE 1

Pharmacokinetic parameter estimates of PF02341066 in athymic mice bearing GTL16 or U87MG tumors after repeated oral administration of PF02341066

Precision of the estimates is expressed as S.E. in parentheses.

Study	Dose	k_a	CL/F	V/F
	mg/kg	h^{-1}	*liters/h/kg*	*liters/kg*
PKPD 1	8.5	0.291 (0.014)	9.23 (1.46)	32.0 (5.9)
	17	0.282 (0.014)	4.70 (0.95)	16.6 (4.1)
	34	0.300 (0.026)	1.53 (0.40)	3.23 (3.13)
PKPD 2	6.25	0.238 (0.012)	13.6 (1.9)	56.0 (9.9)
	12.5	0.336 (0.013)	2.71 (0.57)	8.02 (2.30)
	25	0.326 (0.014)	2.38 (0.35)	7.25 (1.29)
	50	0.331 (0.018)	1.80 (0.17)	5.56 (0.68)
PKPD 3	6.25	0.248 (0.016)	7.83 (1.10)	31.6 (4.8)
	12.5	0.240 (0.018)	3.11 (0.24)	5.04 (1.22)
	25	0.238 (0.015)	2.83 (0.16)	3.32 (0.75)
	50	0.242 (0.010)	1.98 (0.18)	2.49 (0.52)

PKPD 1 and 2, athymic mice bearing GTL16 human gastric carcinoma; PKPD 3, athymic mice bearing U87MG human glioblastoma; k_a, absorption rate constant; CL/F, oral clearance; V/F, oral volume of distribution.

estimated to be 19 ng/ml (Table 2). The calculated EC_{90} value by the Hill equation was 167 ng/ml. The final parameter estimates from the bootstrap validation of the link model were 19 ng/ml (10th and 90th percentiles: 15 and 22 ng/ml, respectively) for EC_{50} and 0.13 h^{-1} (0.11 and 0.16 h^{-1}, respectively) for k_{e0}. The final parameter estimates from the bootstrap validation of the indirect response model with the effect compartment were 19 ng/ml (16 and 21 ng/ml, respectively) for EC_{50}, 20.2 h^{-1} (19.7 and 20.7 h^{-1}, respectively) for k_{out} and 0.14 h^{-1} (0.11 and 0.16 h^{-1}, respectively) for k_{e0}. Thus, the final parameter estimates (50th percentile) for the bootstrap validation were in good agreement with the estimates of the final model ($<\pm 2\%$).

Regarding the tumor growth inhibition, the antitumor efficacies of PF02341066 on day 11 (the last dosing day) in the GTL16 xenograft model were 25, 34, 60, 89, and 100% inhibition at the doses of 3.13, 6.25, 12.5, 25, and 50 mg/kg, respectively (Zou et al., 2007). The antitumor efficacies of PF02341066 on day 9 (the last dosing day) in the U87MG xenograft model were 35, 50, 71, 83, and 97% inhibition at the doses of 3.13, 6.25, 12.5, 25, and 50 mg/kg, respectively (Zou et al., 2007). The observed and model-fitted tumor volume-time profiles in athymic mice implanted with GTL16 and U87MG xenografts are graphically presented in Figs. 5 and 6, respectively. The exponential tumor growth model including the growth rate inhibition by PF02341066 concentration well fitted the individual tumor volume-time profiles of the GTL16 and U87MG xenografts during the PF02341066 repeated-dose treatment. The objective function values for the GTL16 and U87MG xenograft models were 2404 and 2514, respectively. The EC_{50} values were estimated to be 213 ng/ml (17 nM free) in the GTL16 model and 94 ng/ml (7.5 nM free) in the U87MG model (Table 3). The final parameter estimates of EC_{50} for the bootstrap validation were 214 ng/ml (10th and 90th percentiles: 58 and 370 ng/ml, respectively) for the GTL16 xenograft model and 95 ng/ml (28 and 161 ng/ml, respectively) for the U87MG xenograft model. The final parameter estimates of all the PKPD parameters were in good agreement with the estimates of the final model ($<\pm 1\%$).

Discussion

The present study provides novel information on the PKPD relationship for an orally available cMet kinase inhibitor in human tumor xenograft models. The pharmacodynamic biomarker response, measured as cMet phosphorylation, was delayed relative to the plasma concentrations of PF02341066 in the tumor xenografts models. Slow distribution to tumors may be one of the reasons for this delayed response (hysteresis). This observation therefore positioned PF02341066 as an interesting compound to investigate the application of two types of PKPD models that have been proposed to characterize the delay between drug concentration and biomarker response, that is, the link model (Sheiner et al., 1979) and the indirect response model (Dayneka et al., 1993; Jusko et al., 1994). In the link model, it is assumed that the rate of onset and offset of biomarker response is governed by the rate of drug distribution to and from a hypothetical "effect site" (Sheiner et al., 1979). However, many drugs showed delayed response for other reasons, particularly because of indirect mechanisms of action such as stimulation or inhibition of formation (k_{in}) or loss (k_{out}) of substance controlling the physiological response (Dayneka et al., 1993; Jusko et al., 1994). The indirect response model accounts for delays caused by the time needed for changes in k_{in} or k_{out} to be fully expressed in the measured physiological response. In

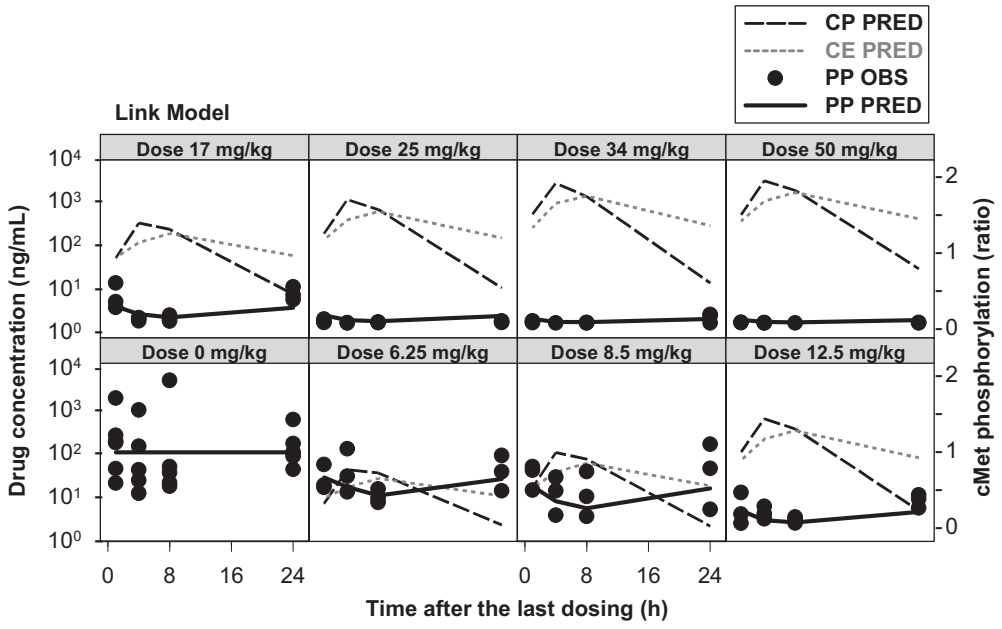

FIG. 3. Observed and model-fitted cMet phosphorylation inhibition by PF02341066 in athymic mice implanted with GTL16 xenografts after repeated oral administration of PF02341066 (link model). CP PRED, model-fitted plasma concentrations of PF02341066; CE PRED, model-fitted concentrations of PF02341066 in the effect compartment; PP OBS, observed cMet phosphorylation (ratio to the mean of control animals), PP PRED, model-fitted cMet phosphorylation (ratio to the mean of control animals).

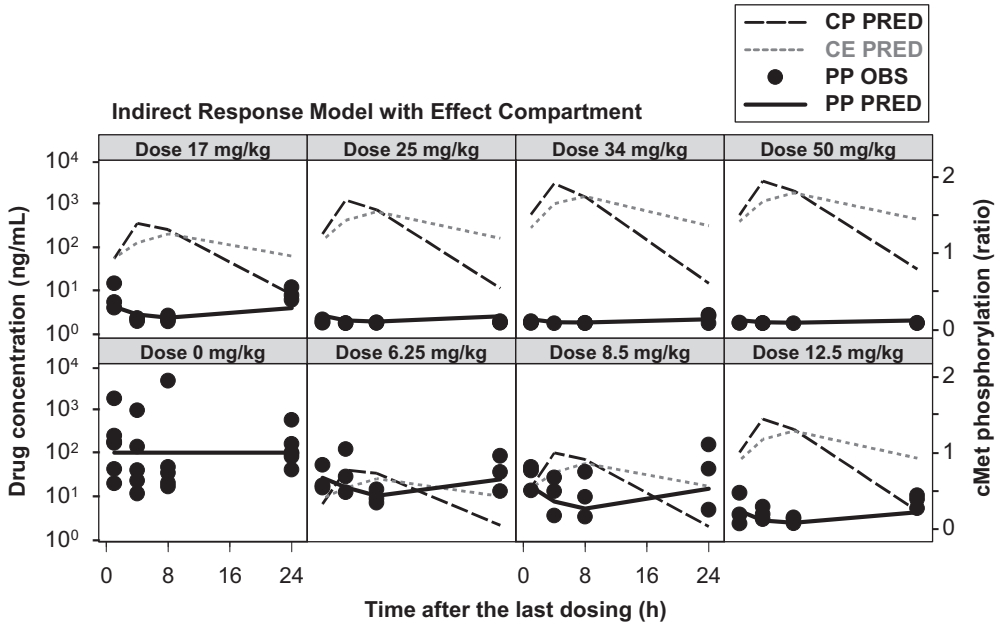

FIG. 4. Observed and model-fitted cMet phosphorylation inhibition by PF02341066 in athymic mice implanted with GTL16 xenografts after repeated oral administration of PF02341066 (indirect response model with effect compartment). CP PRED, model-fitted plasma concentrations of PF02341066; CE PRED, model-fitted concentrations of PF02341066 in the effect compartment; PP OBS, observed cMet phosphorylation (ratio to the mean of control animals), PP PRED, model-fitted cMet phosphorylation (ratio to the mean of control animals).

the present study, the link model provided adequate fitting for the inhibition of cMet phosphorylation (objective function value = −322). On the contrary, the indirect response model did not fit the cMet phosphorylation time course well (objective function value = −266). We therefore incorporated the effect compartment into the indirect response model, resulting in better fitting for the inhibition of cMet phosphorylation (objective function value = −322). The pharmacodynamic parameters obtained from this combined model, that is, the indirect response model with the effect compartment, were identical to those from the link model: EC_{50} = 19 ng/ml and k_{e0} = 0.14 h^{-1} (Table 2). The objective function values for both the models were also identical. In the combined model, k_{out} was estimated to be 20 h^{-1}, which was much larger than the estimated k_{e0} (0.14 h^{-1}), representing essentially instantaneous equilibration of cMet phosphorylation in response to changes in the drug concentration. The estimate of k_{e0} was equivalent to a drug distribution half-life of 5 h. Consistently PF02341066 showed a relatively large volume of

TABLE 2

Pharmacodynamic parameter estimates of PF02341066 for cMet phosphorylation in athymic mice bearing GTL16 tumors after repeated oral administration of PF02341066

Precision of the estimates is expressed as S.E. in parentheses.

Parameters	Link Model	IDR Model	Combined Model
EC_{50} (ng/ml)	18.5 (2.65)	4.59 (0.84)	18.5 (2.72)
E_0	1 fixed	1 fixed	1 fixed
E_{max}	1 fixed	1 fixed	1 fixed
k_{e0} (h^{-1})	0.135 (0.020)	N.A.	0.136 (0.020)
k_{out} (h^{-1})	N.A.	0.159 (0.046)	20.0 (0.8)
OFV	−322	−265	−322

IDR model, indirect response model; combined model, indirect response model with effect compartment; EC_{50}, the concentration causing one-half maximum effect; E_0, the baseline of cMet phosphorylation; E_{max}, maximum effect; k_{e0}, the rate constant for equilibration with the effect site; k_{out}, the degradation rate constant; OFV, the objective function value; N.A., not applicable.

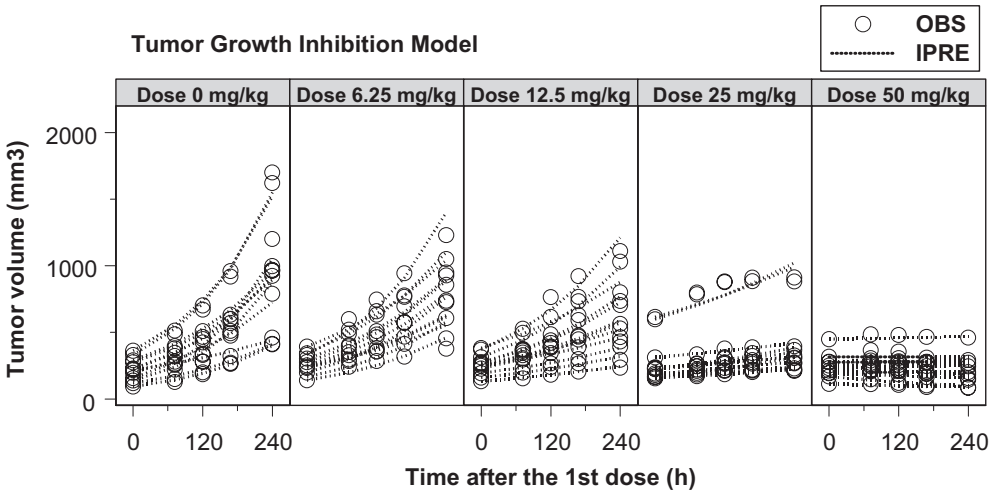

FIG. 5. Observed and model-fitted tumor growth inhibition by PF02341066 in athymic mice implanted with GTL16 xenografts after repeated oral administration of PF02341066. OBS, observed tumor volume; IPRE, model-fitted individual tumor volume.

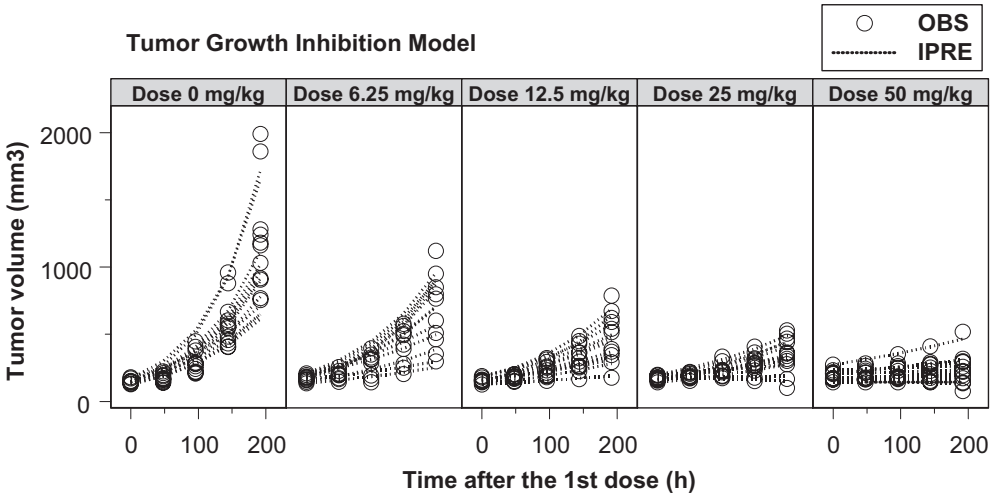

FIG. 6. Observed and model-fitted tumor growth inhibition by PF02341066 in athymic mice implanted with U87MG xenografts after repeated oral administration of PF02341066. OBS, observed tumor volume; IPRE, model-fitted individual tumor volume.

TABLE 3

Pharmacodynamic parameter estimates of PF02341066 for tumor growth inhibition in athymic mice bearing GTL16 or U87MG tumors after repeated oral administration of PF02341066

Precision of the estimates is expressed as S.E. in parentheses.

Parameters	GTL16 Tumor Xenografts	U87MG Tumor Xenografts
EC_{50} (ng/ml)	213 (123)	94.1 (52.3)
E_{max}	1 fixed	1 fixed
k_{in} (h^{-1})	0.0130 (0.00214)	0.0134 (0.00136)
k_{out} (h^{-1})	0.00672 (0.00243)	0.00236 (0.00137)
OFV	2404	2514

EC_{50}, the concentration causing one-half maximum effect; E_{max}, maximum effect; k_{in}, the tumor growth rate constant; k_{out}, the tumor loss rate constant; OFV, the objective function value.

distribution (2.5–56 liters/kg). The maximum plasma concentrations were observed at a relatively late time point, i.e., 4 h postdose (Fig. 2). These pharmacokinetic trends were observed across preclinical species (in-house data). In addition, PF02341066 demonstrated a rapid inhibition of cMet phosphorylation (<20 min) in GTL-16 gastric carcinoma cells in vitro (Zou et al., 2007). These findings taken together suggest that the main reason for the observed hysteresis is a rate-limiting distribution from plasma to the effect site, i.e., tumors. The factors controlling cMet phosphorylation levels might be of no importance to the observed hysteresis. Therefore, the combined model would be better simplified to the link model. This is in line with the theoretical hypothesis that there are circumstances in which the indirect response model could mimic a direct pharmacological response (Jusko et al., 1995; van Schaick et al., 1997). In general, the intermediary components between pharmacokinetics in plasma and the pharmacodynamic response in effect site, such as drug distribution to the effect site, indirect response mechanisms, cascading transduction steps, and others, are not known in advance. For this reason, a general PKPD model combining an indirect response model and effect compartment has been proposed to describe a time delay (hysteresis) between pharmacokinetics in plasma and pharmacodynamic response in effect site (Verotta et al., 1995; Mager et al., 2003). The distinction between the different processes in the combined indirect response model/effect compartment requires intensive sampling at multiple doses in relation to the half-lives of the k_{e0} value and the rate of biosignal turnover. The PKPD field is clearly moving toward mechanistic modeling to have a deeper understanding of the actions of drugs.

We evaluated PKPD relationships of the plasma concentrations of PF02341066 to the inhibition of cMet phosphorylation at steady state after multiple doses of PF02341066. In general, the application of conventional PKPD models assumes that the model parameters stay constant over time. Based on our preliminary studies, no tolerance or sensitization of cMet phosphorylation was observed between single-dose studies and multiple-dose studies. The inhibition of cMet phosphorylation was reversible and returned to the baseline level at the lower dose levels in the present studies. In addition, our pharmacokinetic studies of PF02341066 in rodents did not indicate accumulation and/or induction of PF02341066 plasma concentrations. There-

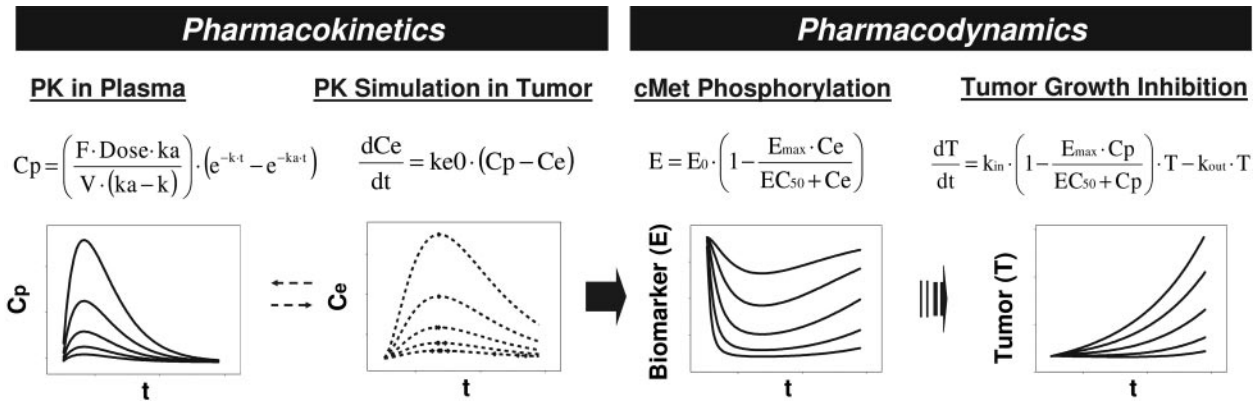

FIG. 7. PKPD modeling summary of cMet phosphorylation inhibition and anti-tumor efficacy by PF02341066 in human tumor xenograft models.

fore, it was not necessary to incorporate time-dependent parameters to the present PKPD models.

It has long been recognized that in vivo tumor growth in xenograft models follows exponential growth in its early phases, subsequently follows a linear growth, and eventually reaches a plateau (Gompertz, 1825; Bissery et al., 1996). This inhibition is mainly reflected by the fact that a large tumor mass hampers the nutrient supply. Such growth curves can be described by a Gompertz model (Gompertz, 1825). However, a plateau phase is never observed in general xenograft model data sets. Therefore, some mathematical models have been proposed to characterize an exponential growth followed by a linear kinetics (Norton and Simon, 1977; Simeoni et al., 2004). In the present study, the exponential tumor growth inhibition model was used to quantitatively determine EC_{50} estimates of PF02341066. We first performed the exponential tumor growth model analysis, in which the first-order growth rate (k_{in}) was inhibited by both the PF02341066 concentration and the tumor volume expressed as TG_{50}, which inhibited 50% of the tumor growth rate. The TG_{50} values for the GTL16 and U87MG xenograft models were estimated to be greater than 10,000 mm^3, which was much larger than the observed maximum tumor volumes. The model-fitted tumor growth curves in the GTL16 and U87MG xenograft models were superimposed between the two models with and without the TG_{50} estimation. The PKPD model was therefore simplified to the exponential tumor growth model without TG_{50}. That is, the tumor growth rate was inhibited by only the PF02341066 concentration. Thus, the present approach is flexible enough to accurately characterize the growth patterns of different cell lines in xenograft models.

Regarding the biomarker-pharmacological response relationships between cMet phosphorylation and antitumor efficacy, the following relationships were apparently characterized: 1) the complete inhibition of cMet phosphorylation during the dosing interval, i.e., 24 h, was consistent with the complete tumor growth inhibition and 2) potent inhibition of cMet phosphorylation for only a portion of the dosing interval was consistent with suboptimal antitumor efficacy. In the present PKPD analyses, these findings were also characterized in a quantitative manner using the PKPD modeling for biomarker response and tumor growth inhibition. The PKPD results in the GTL16 xenograft model suggested that the EC_{50} value for tumor growth inhibition (213 ng/ml total) was equivalent to the EC_{90} value for cMet phosphorylation (167 ng/ml total). In addition, a similar dose-dependent effect of PF02341066 on cMet phosphorylation at 4 h postdose and tumor growth inhibition was observed in the U87MG xenograft model (Zou et al., 2007). The EC_{50} values for tumor growth inhibition were similar between the GTL16 (213 ng/ml total) and U87MG (94 ng/ml total) xenograft models (Table 3). The pharmacokinetic parameters of PF02341066 were also similar between the GTL16 and U87MG xenograft models (Table 1; Fig. 2). Collectively these findings suggest that the duration of cMet phosphorylation inhibition is important to maximize antitumor efficacy of PF02341066.

In conclusion, the PKPD relationship of the plasma concentrations of PF02341066 to the inhibitions of cMet phosphorylation and tumor growth in human tumor xenografts models were well characterized in a quantitative manner using the PKPD modeling described in the present study (Fig. 7). That is, the EC_{90} value (167 ng/ml) for the inhibition of cMet phosphorylation corresponded to the EC_{50} value (213 ng/ml) for the GTL16 tumor growth inhibition, suggesting that near-complete inhibition of cMet phosphorylation (>90%) is required to significantly inhibit tumor growth (>50%). Therefore, the EC_{90} value for the inhibition of cMet phosphorylation could be considered to be the minimum target efficacious concentration in the clinic. The PKPD modeling results also provide insights in the factor that determines the time course of the inhibition of cMet phosphorylation. That is, the distribution process of PF02341066 to target tissues could be a rate-limiting step in the pharmacodynamics of PF02341066. On the basis of the present preclinical PKPD modeling, an efficacious clinical dose of PF02341066 could be projected with accurately predicted or pharmacokinetic parameters obtained in patients by simulating near-complete inhibition of cMet phosphorylation (>90%) with the target efficacious concentrations. The present PKPD results will be helpful in determining the appropriate dosing regimen and in guiding dose escalation to rapidly achieve efficacious systemic exposure in the clinic.

Acknowledgments. We acknowledge the expert technical assistance of members of the PK Group (Pfizer Global Research and Development, San Diego, CA), Melissa Cook and Robert Hunter, for the animal experiments. We also thank Jean Cui, Michelle Tran-Dube, Pei-Pei Kung, and Mitch Nambu (Pfizer Global Research and Development) for synthesizing PF02341066.

References

Beal SL and Sheiner LB (1992) *NONMEM User Guides,* University of California at San Francisco, San Francisco, NONMEM Project Group.

Bellusci S, Moens G, Gaudino G, Comoglio P, Nakamura T, Thiery JP, and Jouanneau J (1994) Creation of an hepatocyte growth factor/scatter factor autocrine loop in carcinoma cells induces invasive properties associated with increased tumorigenicity. *Oncogene* **9:**1091–1099.

Birchmeier C, Birchmeier W, Gherardi E, and Vande Wound GF (2003) Met, metastasis, motility and more. *Nat Rev Mol Cell Biol* **4:**915–9125.

Bissery MC, Vrignaud P, Lavelle F, and Chabot GG (1996) Experimental antitumor activity and pharmacokinetics of camptothecin analog irinotecan (CPT-11) in mice. *Anticancer Drugs* **7:**437–460.

Chien JY, Friedrich S, Heathman MA, de Alwis DP, and Sinha V (2005) Pharmacokinetics/pharmacodynamics and the stages of drug development: role of modeling and simulation. *AAPS J* **7:**E544–E559.

Dayneka NL, Garg V, and Jusko WJ (1993) Comparison of four basic models of indirect pharmacodynamic responses. *J Pharmacokinet Biopharm* **21:**457–478.

Derendorf H , Lesko LJ, Chaikin P, Colburn WA, Lee P, Miller R, Powell R, Rhodes G, Stanski D, and Venitz J (2000) Pharmacokinetic/pharmacodynamic modeling in drug research and development. *J Clin Pharmacol* **40:**1399–1418.

Efron B and Tibshirani R (1993) *An Introduction to the Bootstrap,* London, Chapman & Hall.

Gompertz B (1825) On the nature of the function expressive of the law of human mortality, and on the new mode of determining the value of life contingencies. *Phil Trans R Soc Lond* **115:**513–585.

Jeffers M, Schmidt L, Nakaigawa N, Webb CP, Weirich G, Kishida T, Zbar B, and Vande Woude GF (1997) Activating mutations for the Met tyrosine kinase receptor in human cancer. *Proc Natl Acad Sci U S A* **94:**11445–11450.

Jusko WJ and Ko HC (1994) Physiologic indirect response models characterize diverse types of pharmacodynamic effects. *Clin Pharmacol Ther* **56:**406–419.

Jusko WJ, Ko HC, and Ebling WF (1995) Convergence of direct and indirect pharmacodynamic response models. *J Pharmacokinet Biopharm* **23:**5–8.

Lesko LJ, Rowland M, Peck CC, and Blascheke TF (2000) Optimizing the science of drug development: opportunities for better candidate selection and accelerated evaluation in humans. *Pharm Res* **17:**1335–1344.

Mager DE, Wyska E, and Jusko WJ (2003) Diversity of mechanism-based pharmacodynamic models. *Drug Metab Dispos* **31:**510–518.

Norton L and Simon R (1977) Growth curve of an experimental solid tumor following radiotherapy. *J Natl Cancer Inst* **58:**1735–1741.

Rong S, Bodescot M, Blair D, Dunn J, Nakamura T, Mizuno K, Park M, Chan A, Aaronson S, and Vande Woude GF (1992) Tumorigenicity of the met proto-oncogene and the gene for hepatocyte growth factor. *Mol Cell Biol* **12:**5152–5158.

Rong S, Segal S, Anver M, Resau JH, and Vande Woude GF (1994) Invasiveness and metastasis of NIH 3T3 cells induced by Met-hepatocyte growth factor/scatter factor autocrine stimulation. *Proc Natl Acad Sci U S A* **91:**4731–4735.

Sheiner LB (1984) The population approach to pharmacokinetic data analysis: rational and standard data analysis methods. *Drug Metab Rev* **15:**153–171.

Sheiner LB, Stanski DR, Vozeh S, Miller RD, and Ham J (1979) Simultaneous modeling of pharmacokinetics and pharmacodynamics: application to *d*-tubocurarine. *Clin Pharmacol Ther* **25:**358–371.

Simeoni M, Magni P, Cammia C, De Nicolao G, Croci V, Pesenti E, Germani M, Poggesi I, and Rocchetti M (2004) Predictive pharmacokinetic-pharmacodynamic modeling of tumor growth kinetics in xenograft models after administration of anticancer agents. *Cancer Res* **64:**1094–1101.

van Schaick EA, De Graaf HJMM, IJzerman AP, and Danhof M (1997) Physiological indirect effect modeling of the anti-lipolytic effects of adenosine A1 receptor agonists. *J Pharmacokinet Biopharm* **25:**713–730.

Verotta D and Sheiner LB (1995) A general conceptual model for non-steady-state pharmacokinetic/pharmacodynamic data. *J Pharmacokinet Biopharm* **23:**1–4.

Zou HY, Li Q, Lee J, Arango M, McDonnell SR, Dusell C, Stempniak M, Yamazaki S, Koudriakova T, Alton G, et al. (2007) An orally available small molecule inhibitor of cMet, PF-2341066, exhibits cytoreductive antitumor efficacy through antiproliferative and antiangiogenetic mechanisms. *Cancer Res* **67:**4408–4417.

Address correspondence to: Dr. Shinji Yamazaki, Pharmacokinetics, Dynamics and Metabolism, La Jolla Laboratories, Pfizer Global Research and Development, 10777 Science Center Dr., San Diego, CA 92121. E-mail: shinji.yamazaki@pfizer.com

0090-9556/10/3809-1436–1442$20.00
DRUG METABOLISM AND DISPOSITION
Vol. 38, No. 9
32912/3616055
Printed in U.S.A.

DMD 38:1436–1442, 2010

Pharmacokinetic-Pharmacodynamic Modeling of Tumor Growth Inhibition and Biomarker Modulation by the Novel Phosphatidylinositol 3-Kinase Inhibitor GDC-0941

Laurent Salphati, Harvey Wong, Marcia Belvin, Delia Bradford, Kyle A. Edgar, Wei Wei Prior, Deepak Sampath, and Jeffrey J. Wallin

Departments of Drug Metabolism and Pharmacokinetics (L.S., H.W., D.B.), Cancer Signaling (M.B., K.A.E., J.J.W.), and Translational Oncology (W.W.P., D.S.), Genentech, Inc., South San Francisco, California

Received February 23, 2010; accepted June 10, 2010

ABSTRACT:

The phosphatidylinositol 3-kinase (PI3K) pathway is a major determinant of cell cycling and proliferation. Its deregulation, by activation or transforming mutations of the p110α subunit, is associated with the development of many cancers. 2-(1*H*-Indazol-4-yl)-6-(4-methanesulfonyl-piperazin-1-ylmethyl)-4-morpholin-4-yl-thieno[3,2-*d*]pyrimidine (GDC-0941) is a novel small molecule inhibitor of PI3K currently being evaluated in the clinic as an anticancer agent. The objectives of these studies were to characterize the relationships between GDC-0941 plasma concentrations and tumor reduction in MCF7.1 breast cancer xenografts and to evaluate the association between the tumor pharmacodynamic biomarker [phosphorylated (p) Akt and phosphorylated proline-rich Akt substrate of 40 kDa (pPRAS40)] responses and antitumor efficacy. MCF7.1 tumor-bearing mice were treated for up to 3 weeks with GDC-0941 at various doses (12.5–200 mg/kg) and dosing schedules (daily to weekly). An indirect response model fitted to tumor growth data indicated that the GDC-0941 plasma concentration required for tumor stasis was approximately 0.3 μM. The relationship between GDC-0941 plasma concentrations and inhibition of pAkt and pPRAS40 in tumor was also investigated after a single oral dose of 12.5, 50, or 150 mg/kg. An indirect response model was fitted to the inhibition of Akt and PRAS40 phosphorylation data and provided IC_{50} estimates of 0.36 and 0.29 μM for pAkt and pPRAS40, respectively. The relationship between pAkt inhibition and tumor volume was further explored using an integrated pharmacokinetic biomarker tumor growth model, which showed that a pAkt inhibition of at least 30% was required to achieve stasis after GDC-0941 treatment of the MCF7.1 xenograft.

Introduction

The phosphatidylinositol 3-kinase (PI3K) pathway plays a major role in cell survival, motility, differentiation, and metabolism (Engelman et al., 2006). As part of this pathway, the PI3K family of lipid kinases catalyzes the phosphorylation of the 3′-hydroxyl group of phosphatidylinositols, leading to the activation of the serine/threonine protein kinase Akt and further downstream effectors, such as PRAS40, part of the mTOR complex 1, and S6 kinases (Engelman, 2009). The PI3Ks are divided into three classes based on their substrate specificity and sequence homology; in class I, four isoforms of the catalytic subunit p110 have been identified. The α and β isoforms, belonging to class IA, are ubiquitously expressed, whereas the δ and γ isoforms, belonging to class IA and IB, respectively, are mainly present in leukocytes (Ghigo and Hirsch, 2008). Over the past few years, numerous mutations, leading to the deregulation of the pathway, have been associated with the development of cancers. Activating mutations of the p110α subunit have been noted in breast, colon, prostate, and ovarian cancers (Engelman, 2009; Wong et al., 2010). In addition, mutations or loss of the phosphatase and tensin homolog have also been identified in a large variety of cancers (Chalhoub and Baker, 2009). Thus, the PI3K pathway has emerged as a major target in the development of small molecule anticancer drugs, including the PI3K inhibitors *N*-(3-(benzo[*c*][1,2,5]thiadiazol-5-ylamino)quinoxalin-2-yl)-4-methylbenzenesulfonamide (XL147), 5-(2,6-dimorpholinopyrimidin-4-yl)-4-(trifluoromethyl)pyridin-2-amine (BKM120), and (*Z*)-5-((4-(pyridin-4-yl)quinolin-6-yl)methylene)thiazolidine-2,4-dione (GSK1059615) and dual PI3K/mTor inhibitors (Liu et al., 2009).

GDC-0941 (Fig. 1) is a novel small molecule inhibitor of PI3K currently being evaluated in phase I studies as an anticancer agent. This compound was shown to be selective for the class I PI3K against a panel of 228 kinases (Folkes et al., 2008). Of the kinases tested, only two, the human tyrosine kinase Flt3 and the human kinase TrkA, were inhibited

Article, publication date, and citation information can be found at http://dmd.aspetjournals.org.
doi:10.1124/dmd.110.032912.

ABBREVIATIONS: PI3K, phophatidylinositol 3-kinase; PRAS40, proline-rich Akt substrate of 40kDa; mTor, mammalian target of rapamycin; XL147, *N*-(3-(benzo[*c*][1,2,5]thiadiazol-5-ylamino)quinoxalin-2-yl)-4-methylbenzenesulfonamide; BKM120, 5-(2,6-dimorpholinopyrimidin-4-yl)-4-(trifluoromethyl)pyridin-2-amine; GSK1059615, (*Z*)-5-((4-(pyridin-4-yl)quinolin-6-yl)methylene)thiazolidine-2,4-dione; GDC-0941, 2-(1*H*-indazol-4-yl)-6-(4-methanesulfonyl-piperazin-1-ylmethyl)-4-morpholin-4-yl-thieno[3,2-*d*]pyrimidine; PK, pharmacokinetic; PD, pharmacodynamic; MCT, 0.5% methylycellulose/0.2% Tween 80; TGI, tumor growth inhibition; TV, tumor volume; p, phosphorylated; PF02341066, (*R*)-3-[1-(2,6-dichloro-3-fluoro-phenyl)-ethoxy]-5-(1-piperidin-4-yl-1*H*-pyrazol-4-yl)-pyridin-2-ylamine.

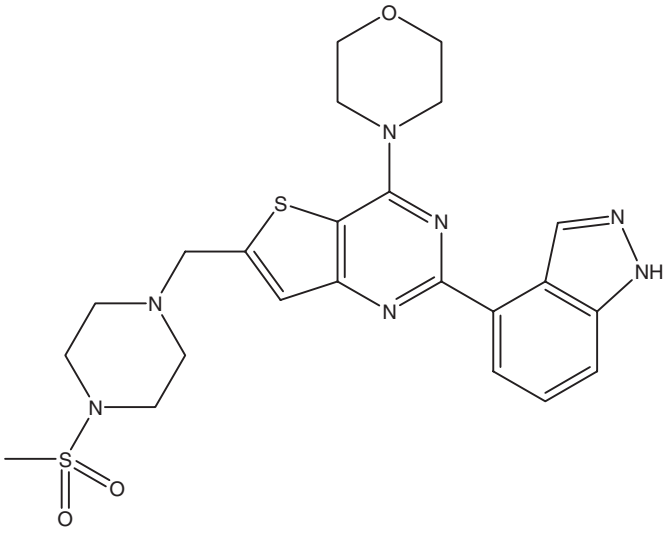

FIG. 1. Chemical structure of GDC-0941.

by more than 50% with 1 μM GDC-0941 (59 and 61%, respectively). GDC-0941 can be considered equipotent against the four class I PI3K isoforms with IC_{50} values of 0.003, 0.033, 0.003, and 0.075 μM against p110α, β, δ, and γ, respectively, and potently inhibits the phosphorylation of Akt in PC3-NCI (prostate) and MCF7.1 cells (breast), with IC_{50} values ranging from 0.028 to 0.037 μM. It is also able to inhibit the proliferation of MCF7.1 and PC3-NCI cells with IC_{50} values of 0.72 and 0.28 μM, respectively (Folkes et al., 2008), and was shown to be efficacious against the U87MG glioblastoma and IGROV-1 human ovarian cancer xenograft models in athymic mice (Raynaud et al., 2009).

Pharmacokinetic (PK)-pharmacodynamic (PD) modeling in preclinical settings can be a valuable tool to explore and understand the relationships between the pharmacokinetic properties of a compound and the PD marker modulation and efficacy data. Once established in preclinical models, these relationships may be useful in assessing the viability of a compound for further development and can be extrapolated to determine potential efficacious levels in humans (Chien et al., 2005) or guide dose escalation in clinical studies.

The objectives of the present studies were to characterize the in vivo efficacy of GDC-0941 and to investigate the PK-PD relationship of the GDC-0941 plasma concentration to MCF7.1 tumor reduction and PD marker (Akt and PRAS40) phosphorylation.

Materials and Methods

Chemicals. GDC-0941 was synthesized by Genentech, Inc. (South San Francisco, CA). All solvents used in analytical assays were from Thermo Fisher Scientific (Waltham. MA) and were of analytical or high-performance liquid chromatography grade. All other chemicals and reagents were purchased from Sigma-Aldrich (St. Louis, MO) unless specified.

Pharmacokinetic Studies. Female athymic nude *nu/nu* mice (Charles River Laboratories, Hollister, CA) weighing 20 to 27 g received oral doses (100 μl) of 5, 50, 75, 100, and 200 mg/kg GDC-0941 in 0.5% methylcellulose-0.2% Tween 80 (MCT). Blood samples (0.2 ml) were collected from each mouse by terminal cardiac puncture at 0.083, 0.25, 0.5, 1, 3, 6, 9, and 24 h postdose into tubes containing K_2EDTA as an anticoagulant. Samples were taken from three different animals at each time point. After the blood was mixed with K_2EDTA, the samples were stored on ice and within 1 h of collection were centrifuged for 5 min at 2000*g* and 2 to 8°C. Plasma was collected and stored at −80°C until analysis. Total concentrations of GDC-0941 were determined by liquid chromatography-tandem mass spectrometry, after plasma protein precipitation with acetonitrile and injection of the supernatant onto the column. A CTC HTS PAL autosampler (LEAP Technologies, Carrboro, NC) linked to a Shimadzu SCL-10A controller with LC-10AD pumps (Shimadzu, Columbia, MD), coupled with a Sciex API 4000 triple quadrupole mass spectrometer (Applied Biosystems, Foster City, CA), was used for the liquid chromatography-tandem mass spectrometry assay. The aqueous mobile phase was water with 0.1% formic acid and the organic mobile phase was acetonitrile with 0.1% formic acid. The total run time was 4 min, and the ionization was conducted in the positive ion mode using the transition m/z 514.3 → 338.2. The internal standard was the deuterated (D8) analog of GDC-0941. The lower and upper limits of quantitation of the assay were 0.005 and 10 μM, respectively.

MCF7.1 Breast Cancer Xenografts Studies. MCF7.1 is an in vivo selected cell line developed at Genentech, Inc. and derived from the parental MCF7 human breast cancer cell line (American Type Tissue Collection, Manassas, VA). Because the tumorigenicity of the MCF7.1 cells in mice is estrogen-dependent, estrogen pellets (17β-estradiol, 0.36 mg/pellet, 60-day release) obtained from Innovative Research of America (Sarasota, FL) were implanted into the dorsal shoulder blade area of female athymic nude *nu/nu* mice. After 3 to 7 days, 20 million human breast cancer MCF7.1 cells, resuspended in a 1:1 mixture of Hanks' buffered salt solution and Matrigel basement membrane matrix (BD Biosciences, San Jose, CA), were subcutaneously implanted into the right flank of each mouse. After implantation, tumors were monitored until they reached a mean tumor volume of 200 to 300 mm^3. Tumor size and body weight were recorded twice per week during the study. Animal body weights were measured using an Adventurer Pro AV812 scale (Ohaus Corporation, Pine Brook, NJ). Tumor lengths and widths were measured using Ultra Cal-IV calipers (model 54-10-111; Fred V. Fowler Company, Inc., Newton, MA). Mice were euthanized if body weight loss was greater than 20% from their initial body weight or if the tumors exceeded 2000 mm^3. The mean tumor volume (TV) across all groups was 269 mm^3 at the initiation of dosing.

Tumor volume was calculated with Excel version 11.2 (Microsoft, Redmond, WA) using the following equation:

$$TV\ (mm^3) = length \times width^2 \times 0.5$$

GDC-0941 was administered orally in MCT for 16 to 21 days. Animals in the control groups received the vehicle, MCT (100 μl). The animals treated with GDC-0941 received the following doses in 100 μl of MCT. Ten mice were assigned to each dose group: experiment 1: vehicle, 12.5, 25, 50, 75, 100, and 200 mg/kg q.d.; experiment 2: vehicle, 12.5, 25, 37.5, 50, and 100 mg/kg b.i.d.; and experiment 3: vehicle, 200 mg/kg q.d., 200 mg/kg every other day, and 200 mg/kg every 3rd day. The tumor volumes at the end of the study for each group were compared with the tumor volume of the corresponding vehicle group.

Mean tumor volumes and S.E.M. were calculated using JMP software (version 5.1.2; SAS Institute, Cary, NC). Statistical analyses of tumor volumes were performed using Dunnett's t test with JMP software.

Modulation of pAKT and pPRAS40 in MCF7.1 Xenografts. Tumor cells were implanted as described previously for the efficacy studies and tumors were monitored until they reached a mean volume of 250 to 350 mm^3. Afterward, the animals were divided into four dose groups and received a single oral dose of vehicle (100 μl of MCT; $n = 7$), 12.5, ($n = 4$), 50 ($n = 4$), or 150 mg/kg ($n = 4$) GDC-0941 in 100 μl of MCT. Tumors were collected at 0.5, 4, 8, and 24 h postdose from the 12.5, 50, and 150 mg/kg treatment groups and at 0.5 ($n = 3$) and 24 h ($n = 4$) postdose from the vehicle group. Excised tumors were flash-frozen and stored at −80°C until analysis.

Frozen tumors were weighed and lysed with a pestle PP (Scienceware, Pequannock, NJ) in cell extract buffer (BioSource, Carlsbad, CA) supplemented with protease inhibitors (F. Hoffman-La Roche, Ltd., Mannheim, Germany), 1 mM phenylmethylsulfonyl fluoride, and phosphatase inhibitor cocktails 1 and 2 (Sigma-Aldrich). Protein concentrations were determined using the BCA Protein Assay Kit (Pierce Chemical, Rockford, IL). The BioSource and Luminex Bio-Plex systems (Bio-Rad Laboratories, Hercules, CA) were used to determine the levels of Akt, phosphorylated at serine 473 (pAkt); PRAS40, phosphorylated at threonine 246 (pPRAS40); and total Akt. These assays quantify protein levels based on measurements of fluorescence intensity. The data were normalized by dividing mean fluorescent values for the pPRAS40 and pAkt Luminex data by the mean fluorescent values of the total Akt Luminex assay.

PK-PD Modeling. PK and PK-PD modeling was performed using SAAMII (Saam Institute, University of Washington, Seattle, WA).

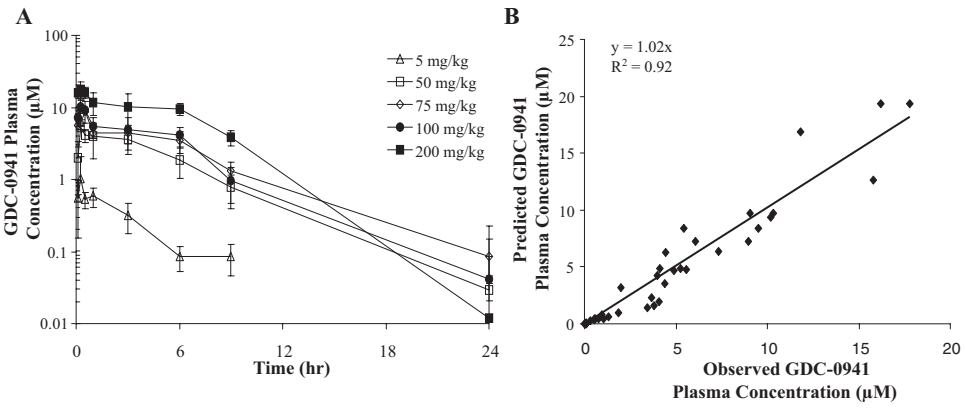

FIG. 2. Pharmacokinetic study in female *nu/nu* mice. A, concentration-time profiles after oral administration of GDC-0941 at 5, 50, 75, 100, and 200 mg/kg. B, observed versus predicted plasma concentrations obtained by fitting a one-compartment model with first order absorption.

Pharmacokinetic analysis. A one-compartment model with first-order oral absorption was used to fit the mean plasma concentration-time data from female *nu/nu* mice. The pharmacokinetics of GDC-0941 appeared linear over the range of doses tested, and the five single doses (5, 50, 75, 100, and 200 mg/kg) were fitted simultaneously. The 40-fold change in dose was associated with an equivalent change in area under the curve between 5 and 200 mg/kg (2.4 μM · h at 5 mg/kg and 115 μM · h at 200 mg/kg). The mean estimates of the absorption rate constant (k_a), the elimination rate constant (k_e), and the apparent volume of distribution (V/F) were used to simulate the GDC-0941 plasma concentrations for the modeling of the xenograft efficacy studies.

Efficacy studies. An indirect response model, described by differential eq. 1, was fitted to the xenograft efficacy data:

$$\frac{d(\mathrm{TV})}{dt} = k_{ng}(\mathrm{TV}) - K(\mathrm{TV}) \quad (1)$$

where t is time (hours), TV is the tumor volume (millimeters cubed), k_{ng} is the net growth rate constant (hour^{-1}), and K is the rate constant (hour^{-1}) associated with the reduction of tumor by GDC-0941. K is further described as

$$K = \frac{K_{max} \times C^n}{KC_{50}^n + C^n}$$

where K_{max} is the maximum value of K (hour^{-1}), C is the plasma concentration of GDC-0941 (micromolar), n is the Hill coefficient, and KC_{50} is the concentration of GDC-0941 where K is 50% of K_{max}.

Blood was collected at a single time point, 1 h postdose at the end (day 21) of the efficacy studies in the q.d. arm (experiment 1). The plasma concentrations determined in these samples (data not shown) were not used further for any analyses or modeling. However, they were similar to the plasma concentrations obtained in the single-dose PK study, indicating the absence of time dependence for the pharmacokinetics of GDC-0941 in mice. Consequently, GDC-0941 plasma concentrations in mice were simulated based on the parameters determined in the pharmacokinetic studies, and mean tumor volumes from each dose group were used in the modeling. The ED_{50} was determined by fixing PD parameter estimates and simulating the daily dose required for 50% reduction of the tumor volume relative to that of the vehicle control group at the end of the study. The plasma concentration needed to achieve tumor stasis was determined when K was equal to k_{ng}.

Modulation of phosphorylation of Akt and PRAS40. The relationship between Akt and PRAS40 phosphorylation in tumors and GDC-0941 plasma concentrations was characterized using an indirect response model, in which the inhibition of the formation of the PD markers pAkt or pPRAS40 by GDC-0941 could be described by eq. 2:

$$\frac{d(\mathrm{PD})}{dt} = k_{in}\left(1 - \frac{C}{\mathrm{IC}_{50} + C}\right) - k_{out}(\mathrm{PD}) \quad (2)$$

where PD corresponds to the level of PD marker (pAkt or pPRAS40) measured (fluorescence intensity), t is time (hours), k_{in} is the rate of formation of the PD marker (fluorescence intensity per hour), C is the plasma concentration of GDC-0941 (micromolar), IC_{50} is the plasma concentration of GDC-0941 producing 50% inhibition of the PD marker (micromolar), and k_{out} (hour^{-1}) is the rate constant defining the loss of the PD marker. Under homeostatic conditions, $k_{in} = k_{out}$ (PD) and k_{out} can be substituted with k_{in}/PD_b, where PD_b represents the level of PD marker at baseline (predose or vehicle control).

GDC-0941 plasma concentrations in mice were simulated based on the parameters determined in the pharmacokinetic studies. Because, as stated above, the plasma concentrations achieved did not seem to markedly change throughout the efficacy study compared with the single-dose PK study, it was assumed that the PD response in the efficacy study could be represented well by the single-dose PD study.

Integrated tumor growth model. To further define the relationship between pAkt inhibition and tumor growth inhibition, the PK-PD model used to characterize the relationship between GDC-0941 plasma concentrations and tumor volumes in the efficacy studies was combined with the model describing the modulation of pAkt. This integrated model assumes that the inhibition of tumor growth is mediated by the decrease in pAkt (i.e., inhibition of phosphorylation of Akt). The changes in pAkt levels were simulated for each dose used in the efficacy study. Thus, the levels of pAkt were related to the tumor volumes using eqs. 3 and 4:

$$\frac{d(\mathrm{TV})}{dt} = k_{ng}(\mathrm{TV}) - K(\mathrm{TV}) \quad (3)$$

where

$$K = \frac{K_{max} \times (\%I)^n}{K(\%I)_{50}^n + (\%I)^n} \quad (4)$$

$\%I$ describes the percentage of inhibition of pAkt and $K(\%I)_{50}$ corresponds to the percentage of inhibition of pAkt where K is 50% of K_{max}. The percentage of inhibition of pAkt needed for tumor stasis was determined when K was equal to k_{ng}.

GDC-0941 plasma concentrations in mice were simulated based on the parameters determined in the pharmacokinetics studies. Mean tumor volumes from all dose groups (experiments 1–3) were fitted simultaneously.

Results

Pharmacokinetic Studies. The pharmacokinetic profiles at the five doses used are presented in Fig. 2A. The parameters k_a, k_e, and V/F were estimated for GDC-0941 after single oral administrations to

TABLE 1

Pharmacokinetic parameters estimated from single oral administration of GDC-0941 to nu/nu mice

Parameter	Estimate	CV
		%
k_a (h^{-1})	10.4	35.4
k_e (h^{-1})	0.23	4.07
V/F (l/kg)	19.9	9.77

CV, coefficient of variation.

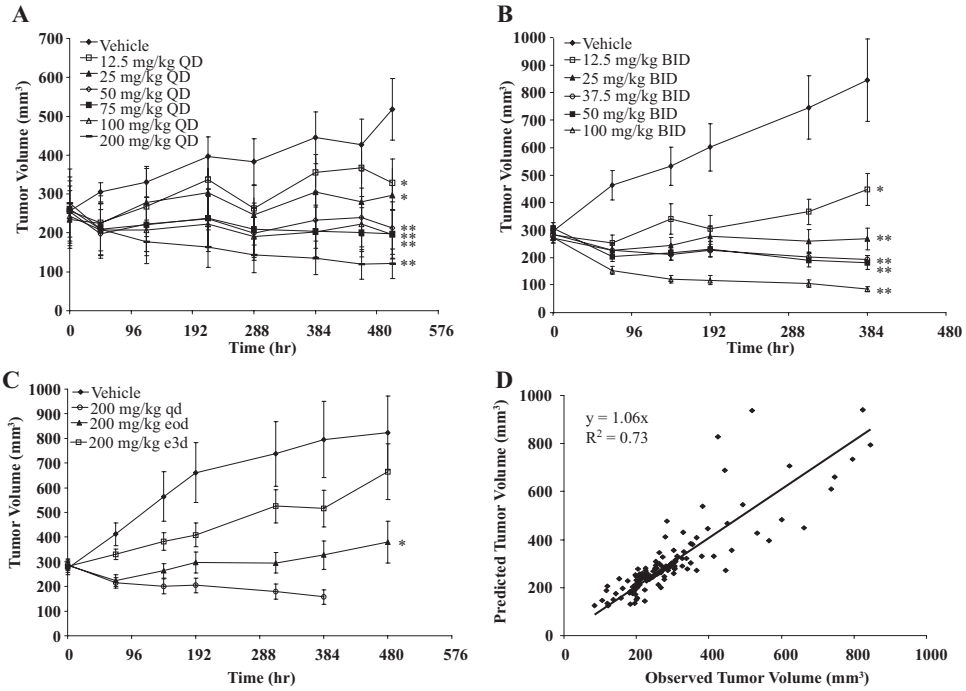

FIG. 3. Xenograft studies in MCF7.1 tumor-bearing mice. Tumor volumes versus time after oral administration of GDC-0941 q.d. (A), b.i.d. (B), or at various dosing schedules (C). D, observed versus predicted tumor volumes obtained by fitting of an indirect response model to all data. No animals could be evaluated at 480 h in the 200 mg/kg q.d. arm because of body weight loss greater than 20%. *, $p < 0.005$; **, $p < 0.0001$. eod, every other day; e3d, every 3rd day.

mice of 5, 50, 75, 100, and 200 mg/kg GDC-0941 in MCT and were 10.4 h^{-1}, 0.23 h^{-1}, and 19.9 l/kg, respectively (Table 1). These estimated parameters were used to simulate plasma concentration-time profiles when the xenograft efficacy and PD marker modulation data were modeled, because serial blood samples adequate for modeling were not collected from tumor-bearing mice during the studies. The comparison between the observed plasma concentrations and model predictions is presented in Fig. 2B and indicates that the PK model used described these data appropriately.

PK-PD Modeling. *Xenograft efficacy studies.* GDC-0941 was administered orally to MCF7.1 tumor-bearing mice at various doses and dosing schedules. Tumor growth inhibition results are presented in Fig. 3, A to C. The inhibition of the MCF7.1 tumor growth appeared to be dose-dependent. Tumor regression was observed at daily doses higher than 50 mg/kg (Fig. 3A) and twice-daily doses higher than 25 mg/kg (Fig. 3B). All doses and regimen showed statistically significant ($p < 0.05$) tumor growth inhibition at the end of the study compared with their respective vehicle group, except the 200 mg/kg every third day (Fig. 3C) treatment group.

An indirect response model was fitted to the tumor data from all studies (eq. 1) and appeared to describe them adequately. The comparison between the observed tumor volumes and model predictions is presented in Fig. 3D. The estimates of the pharmacodynamic parameters describing MCF7.1 tumor growth and reduction effect by GDC-0941 are presented in Table 2.

TABLE 2

Pharmacodynamic parameters estimated from MCF7.1 tumor xenograft studies

Parameter	Estimate	CV
		%
k_{ng} (h^{-1})	0.0027	5.73
K_{max} (h^{-1})	0.0051	4.07
KC_{50} (μM)	0.23	17.5
n	1 (fixed)	
ED_{50} (mg/kg)	16	
C_{stasis} (μM)	0.26	

CV, coefficient of variation.

Modulation of phosphorylation of Akt and PRAS40. The levels of the PD markers pAkt and pPRAS40 were measured in tumors after a single oral administration of GDC-0941 at 12.5, 50, or 150 mg/kg in MCF7.1 tumor-bearing mice. The results are presented in Fig. 4. A sharp decrease in pAkt (Fig. 4A) and pPRAS40 (Fig. 4B) was observed at the three doses, indicative of a potent inhibition of the PI3K pathway. The suppression of the PD markers was pronounced at 30 min postdose and sustained for 8 h at the 50 and 150 mg/kg doses. In contrast, the signal was mostly recovered 4 h postdose at the 12.5 mg/kg dose level. In general, higher GDC-0941 plasma concentrations (simulated) resulted in greater suppression of the PD markers (Fig. 4, A and B).

The comparisons between the observed and predicted pAkt and pPRAS40 levels after fitting with an indirect response model (eq. 2) are presented in Fig. 4, C and D, respectively. The PD parameters are shown in Table 3.

Integrated tumor growth model. The relationship between inhibition of the PI3K pathway and efficacy was further investigated using a PK-PD model integrating GDC-0941 plasma concentrations, pAkt modulation, and tumor growth inhibition (Fig. 5A). The indirect response model describing the relationship between GDC-0941 plasma concentrations and pAkt levels was used to simulate pAkt inhibition for all dose groups included in the efficacy studies. An indirect response model relating the pAkt inhibition to tumor growth inhibition (eqs. 3 and 4) was fitted to the tumor volumes from experiments 1 to 3 simultaneously. The comparison between the observed tumor volumes and model predictions is presented in Fig. 5B, and the estimated parameters are in Table 4. Based on these parameters and the relationship between pAkt inhibition and the rate constant K, representing a tumor reduction effect by GDC-0941 (Fig. 5C), it appeared that a constant inhibition of pAkt of at least 30% would be necessary to achieve tumor stasis. In addition, the simulation of the time course of the pAkt suppression at the daily ED_{50}, based on the parameters

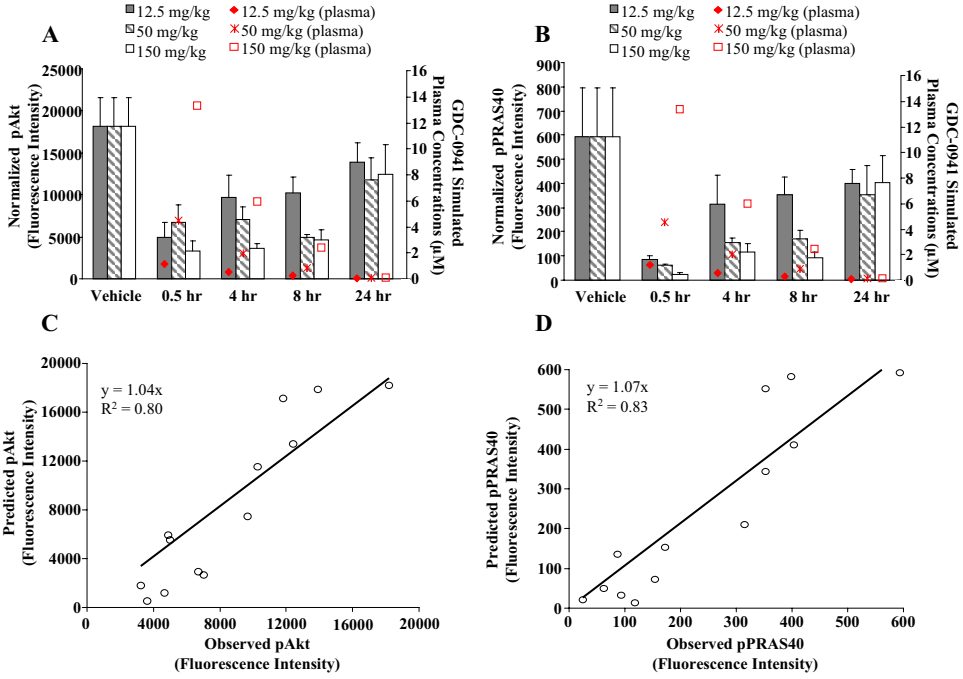

FIG. 4. Levels of pAkt (A) and pPRAS40 (B) in tumors after a single dose of 12.5, 50, or 150 mg/kg GDC-0941 to MCF7.1 tumor-bearing mice. C, observed versus predicted pAkt was obtained by fitting of an indirect response model. D, observed versus predicted pPRAS40 was obtained by fitting of an indirect response model.

listed in Table 3, is presented in Fig. 6. This plot suggests that ~30% inhibition of pAkt is achieved for approximately 10 h at the ED_{50}.

Discussion

The PI3K-Akt pathway is one of the most commonly altered signaling pathways in cancer (Liu et al., 2009). After activation by receptor tyrosine kinases, class I PI3K is recruited to the plasma membrane and converts phosphatidylinositol biphosphate to phosphatidylinositol triphosphate. This initial reaction leads to the activation of the serine/threonine kinase Akt, a major effector of PI3K, which in turn triggers downstream signaling events, including PRAS40 phosphorylation. Mutations of the p110α catalytic subunit of the PI3K have been associated with 27% of breast cancers, 24% of endometrial cancers, and more than 10% of colon and upper digestive tract cancers (Liu et al., 2009). GDC-0941, a selective inhibitor of class I PI3K, is currently being evaluated in clinical trials as an anticancer agent (Sarker et al., 2009).

Indirect response models are relevant when the response measured is the product of an indirect mechanism (Dayneka et al., 1993; Mager et al., 2003), such as the inhibition or stimulation of the formation (k_{in}) or loss (k_{out}) of the mediator controlling the physiological effect. In the present studies, the levels of pAkt and pPRAS40 in tumor were monitored after upstream inhibition of PI3K by GDC-0941 administered as a single dose to MCF7.1 tumor-bearing mice. The inhibition of the production of these two markers (Fig. 3C) was characterized using indirect response models and the in vivo IC_{50} estimates were 0.36 and 0.29 μM for inhibition of pAkt and pPRAS40, respectively (Table 2). For pAkt, this value was approximately 10-fold higher than the IC_{50} measured in vitro (0.028 μM) (Folkes et al., 2008). This difference may be partly explained by the binding to plasma protein in vivo, because GDC-0941 is 97% bound in mouse plasma (E. G. Plise, unpublished data), and/or by limited distribution to the subcutaneous tumor. The IC_{50} for pPRAS40 inhibition was not determined in vitro.

TABLE 3

Pharmacodynamic parameters of GDC-0941 for inhibition of Akt and PRAS40 phosphorylation estimated from a single dose of GDC-0941 in MCF7.1 tumor-bearing mice

Parameter[a]	pAkt	pPRAS40
IC_{50} (μM)	0.36 (25.5)	0.29 (26.0)
k_{in} (fluorescence intensity/h)	89620 (30.5)	4465 (23.9)

[a] Parameters are presented as estimates (% coefficient of variation).

The relationship between GDC-0941 plasma concentrations and MCF7.1 tumor growth inhibition was also adequately described by an indirect response model (Fig. 2). This PK-PD model suggested that GDC-0941 plasma concentrations of approximately 0.3 μM would be necessary to achieve tumor stasis (Table 1), which was comparable to the IC_{50} estimated for both pAkt and pPRAS40 inhibition (Table 2). The similar IC_{50} values established in separate models between GDC-0941 concentrations and inhibition of PD marker phosphorylation or tumor growth imply that approximately 50% inhibition of Akt and PRAS40 phosphorylation would be associated with tumor stasis. This approach, comparing parameters in independent models, was used by Yamazaki et al. (2008) in their investigations of the cMet inhibitor (*R*)-3-[1-(2,6-dichloro-3-fluoro-phenyl)-ethoxy]-5-(1-piperidin-4-yl-1*H*-pyrazol-4-yl)-pyridin-2-ylamine (PF02341066), in which the EC_{90} for the inhibition of cMet phosphorylation was similar to the EC_{50} for tumor growth inhibition, leading the authors to conclude that more than 90% inhibition of cMet phosphorylation would be needed to inhibit tumor growth by more than 50%. We investigated further the relationship between pAkt modulation and tumor growth by using an integrated tumor growth model, as proposed by Wong et al. (2009) and Bueno et al. (2008). This model assumes that tumor growth inhibition is mediated by the decrease in pAkt (Fig. 5A). The curve describing the relationship between inhibition of Akt phosphorylation and tumor growth inhibition, represented by the rate constant *K* (Fig. 5C), indicated that the increase in effect would be less than linear beyond 28.6% inhibition [$K(\%I)_{50}$] and that little improvement in effect would be achieved with pAkt

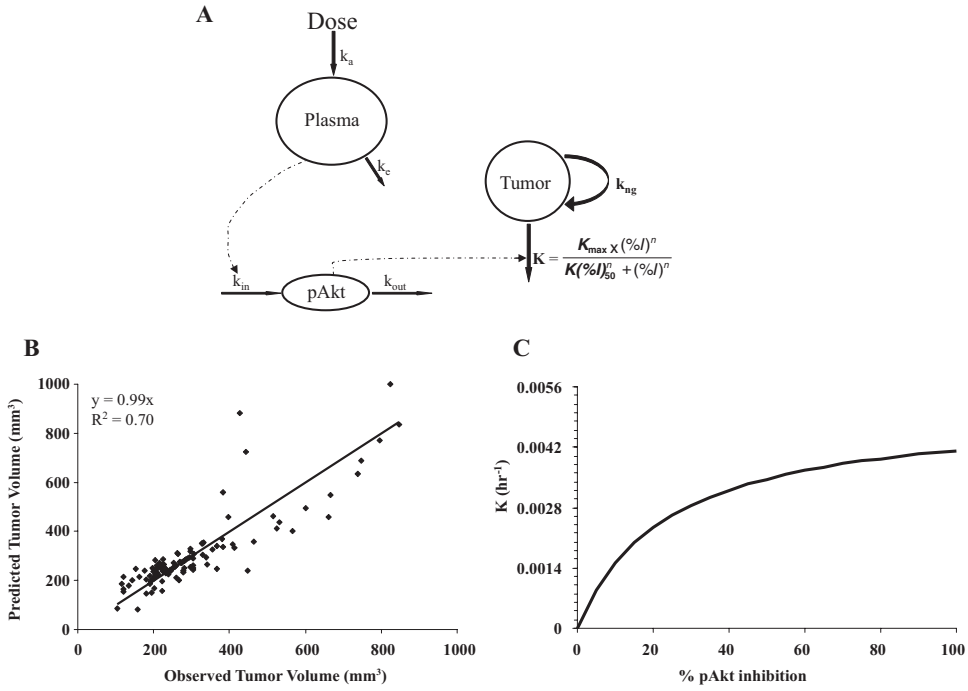

FIG. 5. Integrated tumor growth model linking GDC-0941 plasma concentrations, pAkt inhibition, and tumor growth inhibition. A, parameters estimated [k_{ng}, K_{max}, and $K(\%I)_{50}$] are presented in bold. B, observed versus predicted tumor volumes obtained by fitting the integrated model. C, relationship between percent pAkt inhibition and tumor reduction rate constant K.

inhibition greater than 50%. The modeling also suggested that 30% continuous inhibition of pAkt signal would be required to achieve tumor stasis. This level of pAkt inhibition was achieved for approximately 10 h at the daily ED_{50} of 16 mg/kg (Fig. 6). This is, to our knowledge, the first report describing a PK-PD relationship between modulation of the PI3K pathway and tumor growth inhibition. A similar PK-PD model integrating pPRAS40 modulation and tumor growth inhibition may be built; however, although a decrease in PRAS40 phosphorylation can be considered a marker of the inhibition of the pathway, it remains to be established as a direct driver of tumor growth inhibition (Manning and Cantley, 2007). The integrated model described here may be helpful in trying to predict the likelihood of tumor response in humans from the extent of suppression of the pathway measured by pAkt inhibition. Such an extrapolation assumes that the relationship between PD marker response and antitumor activity is similar in human and xenograft models. The MCF7.1 cells used in these studies harbor a mutation (E545K) of the p110α catalytic subunit, resulting in constitutive PI3K pathway activation (Edgar et al., 2010). Thus, they are considered highly dependent on the pathway, making them sensitive to its inhibition. It is likely that a stronger inhibition of pAkt would be required to achieve stasis of tumor cells less "addicted" to this pathway. However, despite limitations in the translation to human efficacy, the PK-PD modeling performed in the current studies may nevertheless be useful to make "no-go" decisions in compound development, select the optimal times for PD marker data collection, or guide clinical trial design. Such an application was described by Tanaka et al. (2008), who extrapolated the relationship established in rats between the plasma concentrations of everolimus (an mTor inhibitor) and S6 kinase 1 inhibition to simulate the effects of various dosing regimen in human using scaled pharmacokinetics.

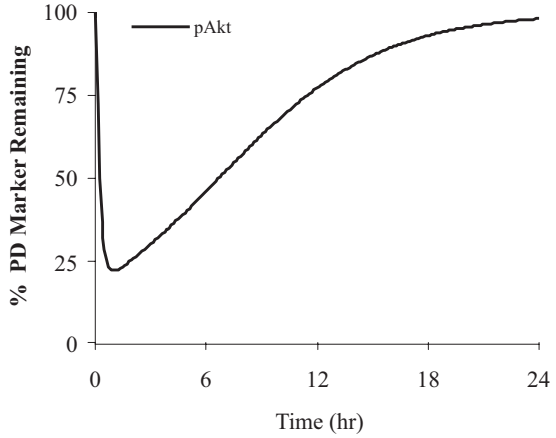

FIG. 6. Simulated time course of pAkt inhibition at ED_{50} (16 mg/kg).

It is also worth noting that the IC_{50} for pAkt estimated preclinically in our model appears consistent with data collected in humans. Dose-dependent inhibition of pAkt measured in platelet-rich plasma was reported in patients, with an IC_{50} that could be estimated to be approximately 0.3 μM (Sarker et al., 2009). Although pAkt was measured in tumor in our studies, this agreement with preliminary clinical data from platelet-rich plasma suggests that the preclinical PK-PD model may be useful in designing future clinical trials.

TABLE 4

Pharmacodynamic parameters of GDC-0941 estimated from fitting the integrated tumor growth model to the efficacy data (experiments 1 to 3)

Parameter	Estimate	CV
		%
k_{ng} (h^{-1})	0.0027	4.13
K_{max} (h^{-1})	0.0053	7.42
$K(\%I)_{50}$ (%)	28.6	24.0
n	1 (fixed)	
pAkt inhibition at stasis (%)	30	

CV, coefficient of variation.

Acknowledgments. We thank the Drug Metabolism and Pharmacokinetics and Translational Oncology Departments and the In Vivo Studies Group for their contributions to the results presented.

References

Bueno L, de Alwis DP, Pitou C, Yingling J, Lahn M, Glatt S, and Trocóniz IF (2008) Semi-mechanistic modelling of the tumour growth inhibitory effects of LY2157299, a new type I receptor TGF-beta kinase antagonist, in mice. *Eur J Cancer* **44:**142–150.

Chalhoub N and Baker SJ (2009) PTEN and the PI3-kinase pathway in cancer. *Annu Rev Pathol* **4:**127–150.

Chien JY, Friedrich S, Heathman MA, de Alwis DP, and Sinha V (2005) Pharmacokinetics/pharmacodynamics and the stages of drug development: role of modeling and simulation. *AAPS J* **7:**E544–E559.

Dayneka NL, Garg V, and Jusko WJ (1993) Comparison of four basic models of indirect pharmacodynamic responses. *J Pharmacokinet Biopharm* **21:**457–478.

Edgar KA, Wallin JJ, Berry M, Lee LB, Prior WW, Sampath D, Friedman LS, and Belvin M (2010) Isoform-specific phosphoinositide 3-kinase inhibitors exert distinct effects in solid tumors. *Cancer Res* **70:**1164–1172.

Engelman JA (2009) Targeting PI3K signalling in cancer: opportunities, challenges and limitations. *Nat Rev Cancer* **9:**550–562.

Engelman JA, Luo J, and Cantley LC (2006) The evolution of phosphatidylinositol 3-kinases as regulators of growth and metabolism. *Nat Rev Genet* **7:**606–619.

Folkes AJ, Ahmadi K, Alderton WK, Alix S, Baker SJ, Box G, Chuckowree IS, Clarke PA, Depledge P, Eccles SA, et al. (2008) The identification of 2-(1*H*-indazol-4-yl)-6-(4-methanesulfonyl-piperazin-1-ylmethyl)-4-morpholin-4-yl-thieno[3,2-*d*]pyrimidine (GDC-0941) as a potent, selective, orally bioavailable inhibitor of class I PI3 kinase for the treatment of cancer. *J Med Chem* **51:**5522–5532.

Ghigo A and Hirsch E (2008) Isoform selective phosphoinositide 3-kinase gamma and delta inhibitors and their therapeutic potential. *Recent Pat Inflamm Allergy Drug Discov* **2:**1–10.

Liu P, Cheng H, Roberts TM, and Zhao JJ (2009) Targeting the phosphoinositide 3-kinase pathway in cancer. *Nat Rev Drug Discov* **8:**627–644.

Mager DE, Wyska E, and Jusko WJ (2003) Diversity of mechanism-based pharmacodynamic models. *Drug Metab Dispos* **31:**510–518.

Manning BD and Cantley LC (2007) AKT/PKB signaling: navigating downstream. *Cell* **129:**1261–1274.

Raynaud FI, Eccles SA, Patel S, Alix S, Box G, Chuckowree I, Folkes A, Gowan S, De Haven Brandon A, Di Stefano F, et al. (2009) Biological properties of potent inhibitors of class I phosphatidylinositide 3-kinases: from PI-103 through PI-540, PI-620 to the oral agent GDC-0941. *Mol Cancer Ther* **8:**1725–1738.

Sarker D, Kristeleit R, Mazina KE, Ware JA, Yan Y, Dresser M, Derynck MA, and de Bono JS (2009) A phase I study evaluating the pharmacokinetics (PK) and pharmacodynamics (PD) of the oral pan-phosphoinositide-3 kinase (PI3K) inhibitor GDC-0941, in *2009 ASCO Meeting*; 2009 May 29–Jun 2; Orlando, FL. 27, abstract 3538, American Society of Clinical Oncology, Alexandria, VA.

Tanaka C, O'Reilly T, Kovarik JM, Shand N, Hazell K, Judson I, Raymond E, Zumstein-Mecker S, Stephan C, Boulay A, et al. (2008) Identifying optimal biologic doses of everolimus (RAD001) in patients with cancer based on the modeling of preclinical and clinical pharmacokinetic and pharmacodynamic data. *J Clin Oncol* **26:**1596–1602.

Wong H, Belvin M, Herter S, Hoeflich KP, Murray LJ, Wong L, and Choo EF (2009) Pharmacodynamics of 2-[4-[(1*E*)-1-(hydroxyimino)-2,3-dihydro-1*H*-inden-5-yl]-3-(pyridine-4-yl)-1*H*-pyraz ol-1-yl]ethan-1-ol (GDC-0879), a potent and selective B-Raf kinase inhibitor: understanding relationships between systemic concentrations, phosphorylated mitogen-activated protein kinase kinase 1 inhibition, and efficacy. *J Pharmacol Exp Ther* **329:**360–367.

Wong KK, Engelman JA, and Cantley LC (2010) Targeting the PI3K signaling pathway in cancer. *Curr Opin Genet Dev* **20:**87–90.

Yamazaki S, Skaptason J, Romero D, Lee JH, Zou HY, Christensen JG, Koup JR, Smith BJ, and Koudriakova T (2008) Pharmacokinetic-pharmacodynamic modeling of biomarker response and tumor growth inhibition to an orally available cMet kinase inhibitor in human tumor xenograft mouse models. *Drug Metab Dispos* **36:**1267–1274.

Address correspondence to: Laurent Salphati, Pharm.D., Ph.D., Genentech, Inc., 1 DNA Way, South San Francisco, CA 94080. E-mail: salphati.laurent@gene.com